

Isotope Dependence of Confinement in JET-ILW Deuterium and Hydrogen Plasmas

H. WEISEN¹, C.F. MAGGI², S. MENMUIR², L. HORVATH³, T.W. BACHE², F.J. CASSON²,
M. OBERPARLEITER⁴, S. SAARELMA², F. AURIEMMA⁵, A. CHANKIN⁴, E. DELABIE⁶,
C. GIROUD², D. KING², R. LORENZINI⁵, E. VIEZZER⁷, P. SIREN⁸, J. VARJE⁹
and JET contributors*

EUROfusion Consortium, JET, Culham Science Centre, Abingdon, OX14 3DB, UK

¹Swiss Plasma Center, Ecole Polytechnique Fédérale de Lausanne, EPFL, Switzerland

Email: henri.weisen@epfl.ch

²CCFE, Culham Science Centre, Abingdon OX14 3DB, UK

³York Plasma Institute, Department of Physics, University of York, York YO10 5DD, UK

⁵Consorzio RFX, Corso Stati Uniti 4, I-35127 Padova, Italy

⁴Max-Planck Institut für Plasmaphysik, D-85748 Garching, Germany

⁶Oak Ridge National Laboratory, Oak Ridge, Tennessee, United States of America

⁷University of Sevilla, Sevilla, Spain

⁸VTT, Espoo, Finland

⁹Aalto University, Espoo, Finland

(*) See the author list of X Litaudon et al. 2017 Nucl. Fusion **57** 102001

Abstract

Heat, particle and momentum confinement in L- and H-mode in deuterium, hydrogen and in D/H mixtures have been investigated in JET with the ITER-like wall (JET-ILW). The paper expands on previous work [1,2] by presenting new results on heat, momentum and particle transport using measured ion temperatures and toroidal rotation frequencies, as well as new gyrokinetic analyses and pedestal studies. In L-mode a weak positive scaling of thermal stored energy with ion mass, $\tau_{\text{Eth}} \propto A^{0.15}$, is found [1], consistently with multi-machine scaling $\tau_{\text{Eth}} \propto A^{0.2}$ [3]. Differences between species in global particle confinement are similarly weak. Core temperature profiles are resilient to changes in input power with $R/L_{\text{Te}} \approx 8$ at mid-radius [1]. Flux-driven core transport modelling with JETTO-TGLF show ITG's to be dominant and predict no isotope scaling as a result of the Ti profile resilience (stiffness), showing that global confinement can depart from simple local GyroBohm scaling. In type I ELMy H-mode it was not possible, except in a couple of cases, to establish the same pedestal and core densities in H as in D, despite gas fuelling rates several times higher in H, showing a strong reduction of global particle confinement in hydrogen. These discharges, too, have stiff temperature profiles with no apparent difference in core R/L_{Te} between species, i.e. differences between species in core and global confinement arise as a result of differences in the pedestal, the most striking of which are differences in pedestal density and pedestal density width. Regressions for the thermal stored energy from kinetic measurements and independently from EFIT equilibrium reconstructions provide mass exponents near 0.4, i.e. twice that of IPB98(y,2). Momentum and particle confinement have a similar strong scaling with isotope mass. Nonlinear GENE gyrokinetic flux-tube calculations at mid-radius, including the effects of collisions, $\omega_{\text{E} \times \text{B}}$ and impurities, show a reversal of GyroBohm scaling in the core of H-modes. Dimensionless identity experiments (identical ρ^*, v^*, β, q) for H and D pairs provided good matches for the kinetic profiles in L-mode and near-identical normalised confinement times, in agreement with JETTO-TGLF modelling [4].

1. INTRODUCTION

Scaling of the plasma confinement properties with the main ion isotope species is of particular importance for predicting JET and ITER performance in deuterium-tritium (D/T) mixtures. For this purpose, JET is engaged in a series of experimental campaigns in order to characterise and understand energy, momentum, particle and impurity confinement and transport in L and H-mode in hydrogen, deuterium and tritium and mixtures thereof [1,2]. Previous work [1] using a database of experiments in deuterium and hydrogen plasmas has shown that L-mode thermal energy confinement scales weakly with atomic mass A , $\tau_{\text{Eth}} \propto A^{0.15}$. In H-mode a scaling as $\tau_{\text{Eth}} \propto A^{0.4}$, significantly stronger than IPB98(y,2) ($\tau_{\text{Eth}} \propto A^{0.19}$) [3], was found, based on kinetic data and assuming $T_i = T_e$. Both of these are ‘anti-GyroBohm’, i.e. have a sign opposite to that expected from simple local GyroBohm scaling ($\tau_{\text{GB}} \propto A^{-0.5}$) [5]. Both L- and H-modes had temperature profiles with nearly identical shapes, i.e. R/L_{Te} exhibited very little variation despite large variations in heat flux, a property we here loosely refer to as ‘profile stiffness’. Interpretive EDGE2D-EIRENE simulations of a pair of matched L-modes in both species were shown to be consistent with a large difference of particle and heat transport in the vicinity of the LCFS [1]. Successful dimensionless identity experiments were performed in L-mode [5], however well matched H-mode pairs in hydrogen and deuterium have not yet been obtained.

The isotope ratio was measured with high resolution Balmer- α spectroscopy and independently using a residual gas analyser [2]. In ‘pure’ isotope conditions, representing the bulk of the data presented here, the H/(H+D), respectively D/(H+D) ratios were typically <2%. T_e and n_e from Thomson scattering (HRTS as used here and LIDAR). T_i , and ω_i were obtained from CXRS (mostly Ne X line and CVI-NeX combinations following diganostics Ne puffs with $n_{Ne}/n_e \sim 0.2\%$, and some CVI only cases). Adequate CXRS data however are only available for approximately half of the dataset. The ion density n_i was inferred from n_e and from Z_{eff} from visible Bremsstrahlung, assuming $Z_{eff}-1$ is due to Be only. Several different ways for inferring the thermal stored energy W_{th} were used for consistency testing, from kinetic data and from the EFIT equilibrium reconstruction after subtraction of the fast ion component $W_{MHD}-W_{fast}$, where the fast ion content was calculated from the PENCIL beam deposition code [6] or, in the presence of ICRH, from the ICRH code PION coupled to PENCIL [7]. PENCIL and PION are also used in the power balance analyses presented in the paper.

2. ISOTOPE DEPENDENCE IN L-MODE

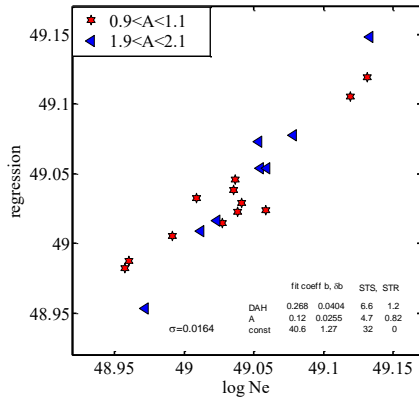


Fig.1 Regression for the total plasma electron content in L-mode. DAH in the legend corresponds to main chamber Balmer alpha emission, A to atomic mass.

The dataset of 20 samples was obtained with $B_T=3$ T, $I_p=2.5$ MA, $\langle n_e \rangle \geq 3.1 \times 10^{19} \text{ m}^{-3}$, $1.5 \text{ MW} \leq P_{NBI} \leq 9.5 \text{ MW}$

It consists of NBI power scans only in hydrogen and deuterium at near constant density ($\pm 10\%$). Divertor strike points were placed on the vertical tiles for highest H-mode power threshold. As a complement to the analysis in [1], which showed $\tau_{Eth} \propto A^{0.15}$, recent charge exchange spectroscopy (CXs) data confirm that $T_i \approx T_e$ and show that the ratio of the momentum-to-energy confinement time is close to unity and slightly lower in hydrogen than in deuterium. The main chamber Balmer alpha emission in hydrogen was ~ 1.2 - 1.5 times higher at the same total electron content $N_e = \int n_e dV$, showing that particle confinement in hydrogen is lower. The scaling of particle confinement is estimated as $N_e \propto A^{0.12} \Gamma_{main}^{0.27}$ or $N_e \propto A^{0.22} \Gamma_{div}^{0.22}$, depending on whether the main chamber emission Γ_{main} or the divertor Balmer alpha emission Γ_{div} is used as a proxy for the particle source. The best regression is obtained with the main chamber emission, shown in fig.1. We hence note that the inferred weak isotope dependence of particle confinement

$\tau_p \propto A^{0.12 \pm 0.03}$ is close to the dependence obtained for energy confinement, $\tau_{Eth} \propto A^{0.15 \pm 0.04}$ [1].

A hydrogen/deuterium pair with \sim same stored energy was predictively modelled under conditions of imposed heat flux using JETTO with the TGLF SAT-1 transport model [8,9]. The boundary conditions, imposed at $\rho=0.85$, were taken from the experimental data. Predicted and experimental profiles, shown in fig.2, are in good agreement for deuterium, less so for hydrogen, for which temperature and density are overpredicted. ITG modes are dominant in the core and the inclusion of E \times B shear in these cases does not lead to an improvement of deuterium confinement relative to hydrogen. The predictions yield nearly the same global confinement time for both species,

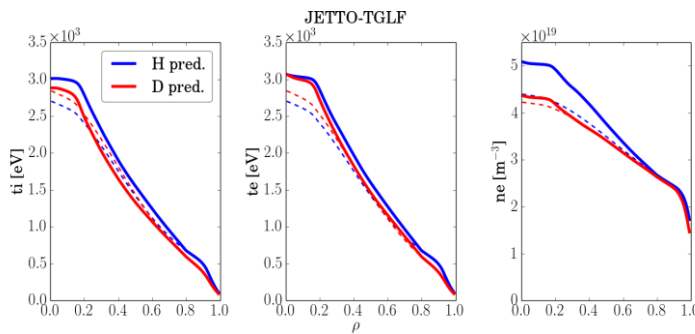


Fig.2 Experimental (dashed lines) and simulated (continuous lines) profiles for hydrogen (blue) and deuterium (red) L-mode discharges with the same stored energy..

i.e. neither GyroBohm scaling, nor weak anti-GyroBohm scaling. This is interpreted as resulting from profile stiffness (high resilience of R/L_T to changes in the heat flux) which is seen in the experiment [1] and is borne out in the simulations. The lesson from this modelling exercise is that several effects can cause a global simulation using an intrinsically local GyroBohm model to deviate from GB scaling, including the boundary conditions, the profile stiffness, the existence of sub-dominant modes in addition to ITG, complex non-linear, zonal flow and multi-scale effects.

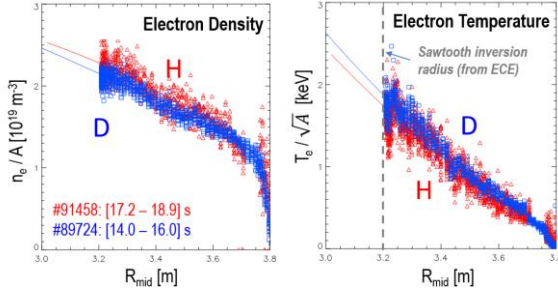


Fig.3 Electron density and temperature profiles for a dimensionless matched pair of hydrogen and deuterium L-mode discharges

scale invariance. The normalised heat diffusivities $A\chi_{\text{eff}}/B_T$ in the confinement zone similar within error bars ($\pm 20\%$). This pair was also predictively simulated using JETTO-TGLF (SAT1), placing the boundary at $\rho=0.8$, agreeing with the experimental T_e and n_e profiles within a few % for both species. There is no significant difference between runs including or excluding the toroidal rotation and E \times B shearing in these low $\beta_N \sim 0.5$ plasmas. These simulations also indicate that the core density peaking results to near 40% from NBI fueling, the remainder being due to the turbulent ITG inward pinch. These identity experiments show that the scale invariance principle is satisfied in the core of these L-modes irrespective of the ion species, i.e. confirm that ρ^* , β , v^* and q are the only significant parameters governing core heat transport in these L-modes. The differences in agreement of JETTO-TGLF for the identity pair and for the pair shown in fig.2 are under investigation. The better agreement for the identity pair may (or should) itself result from the underlying equations satisfying scale invariance.

3. ISOTOPE EFFECT IN TYPE I ELMY H-MODE

Due to the limited NBI power in hydrogen ($\sim 10\text{MW}$), H-mode operation at a unusually low toroidal field for JET was necessary. A ‘‘corner-corner’’ (C/C) configuration, with strike points near the divertor pumping ducts was chosen for best density control and confinement, complemented in a few cases with a vertical/horizontal configuration. The dataset size is 171 samples in total with subsets at $B_T=1\text{T}$, $I_p=1\text{MA}$ ($q_{95} \cong 3$) and $B_T=1.7\text{T}$, $I_p=1.4\text{MA}$ ($q_{95} \cong 3.7$), a few samples at 1.7T, 1.7MA in D only for dimensionless identity experiments. The power range in deuterium: $3.5\text{MW} \leq P_{\text{NBI}} \leq 17\text{MW}$ (only NBI), in hydrogen $5\text{MW} \leq P_{\text{NBI}} \leq 10\text{MW}$, $0 \leq P_{\text{ICRH}} \leq 6.5\text{MW}$. The ICRH power, provided by 2nd harmonic hydrogen heating, was necessary in some hydrogen discharges to access type I ELMY H-modes at the higher field on 1.7T. The experiments consisted mostly in systematic scans of the external gas puff rate and power scans.

Significant progress in the analysis of the H-mode dataset (beyond [1]) was enabled by the provision of CXS data for T_i and toroidal angular frequency ω_ϕ for about half of the dataset. Uncertainties on T_i derived from CXS on impurity lines are significantly higher in JET-ILW due to reduced carbon levels and the appearance of multiple tungsten ‘‘nuisance’’ lines, than they were in JET-C. Consequently all profile data were subjected to a thermal ‘‘equipartition test’’ in order to filter out any data points (about 12% of cases) where the calculated ion-to-electron equipartition power p_{ie} integrated over the volume $Q_{ie} = \int p_{ie} dV$ exceeded the integrated deposited ion source power $Q_{is} = \int p_{is} dV$. A useful way of testing equipartition is to compare the measured ion temperatures to a set fictional ion temperature profiles, dubbed ‘‘equipartition ion temperatures’’, assuming that a certain fraction f_i of the source power is transferred to the electrons by equipartition. The relevant temperature profiles are show for one example in fig.4, for $f_i=0.2, 0.5$ and 1. The same can be done for electrons (f_e -labelled profiles in fig.4, although not relevant to this case), if net equipartition is from the electrons to the ions. Clearly $f_i \geq 1$ is unphysical, as the ions would have zero or negative net heat flux. Fig.4 also shows the CXS impurity temperatures simultaneously inferred from Ne and C in black, the former having been introduced as a tracer (with $n_{\text{Ne}}/n_e \sim 0.2\%$) to improve the measurements. As impurity and main ion temperatures can differ, the main ion temperature (black broken lines in fig.4) has been inferred from the impurity temperatures by a power balance calculation including inter-species equipartition. In the majority of cases $(T_{\text{imp}} - T_{\text{main}})/T_{\text{main}} < 0.03$, although in a handful of cases with high P_{NBI}/n_e , $(T_{\text{imp}} - T_{\text{main}})/T_{\text{main}}$ is as high as 0.05 in the plasma core. This calculation also shows that the temperature differences between impurity species from Be to Ni are negligibly small ($< 0.5\%$), allowing impurity temperature profiles to be combined in a single profile, as here, from several species, without further corrections.

An isotope identity pair in hydrogen and deuterium was achieved at $I_p/B_T = 2.5\text{MA}/3.0\text{T}$ in D and $1.48\text{MA}/1.78\text{T}$ in H, $q_{95} = 3.4$, $\delta = 0.2$, with strike points on divertor vertical targets [5]. In order to keep the ρ^* , β , v^* and q profiles fixed when varying the isotope mass, the plasma parameters must be scaled as $I_p, B_T \propto A^{3/4}$; $n \propto A$ and $T \propto A^{1/2}$ [10]. To satisfy scale invariance [5], the normalised confinement time $\omega_{ci} \tau_{E\text{th}} \propto B_T \tau_{E\text{th}}/A$, a result of the experiment, must be the same, implying that the absorbed input power required to obtain the identity pair, must scale as $P_{\text{abs}} \propto A^{5/4}$. The quality of the match obtained for the scaled T_e and n_e profiles can be gauged from fig.3. The normalised confinement times $B_T \tau_{E\text{th}}/A$ were equal to within 4%, well within the error bars and satisfying

The fact the T_{main} profile in fig.4 is close to the “equipartition ion temperature” calculated for $f_i=0.2$ appears not to be a coincidence. This is shown in fig.5, where against $T_{\text{main}}(\rho)$ is plotted against $T_{\text{ieq}}(f_i=0.2,\rho)$ for three radial positions, $\rho=0.3,0.5$ and 0.7 , showing $T_{\text{main}}(\rho)\approx T_{\text{ieq}}(f_i=0.2,\rho)$ in most cases and for the half of the H-mode dataset for which CXS measurements are available. This allows the hypothesis of equal ion and electron temperatures made in [1] to be replaced by the assumption $T_{\text{main}}(\rho)=T_{\text{ieq}}(f_i=0.2,\rho)$, i.e. by adopting $T_{\text{ieq}}(f_i=0.2,\rho)$ as a surrogate for T_{main} for the purpose of improved confinement regressions.

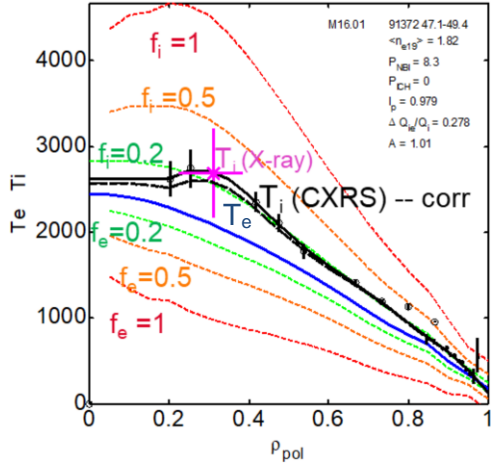


Fig.4 Electron (-), impurity temperature from CXS (-) and main ion temperature (-) profiles in eV inferred from ion/impurity power balance. f_i and f_e labelled profiles are explained in main text.

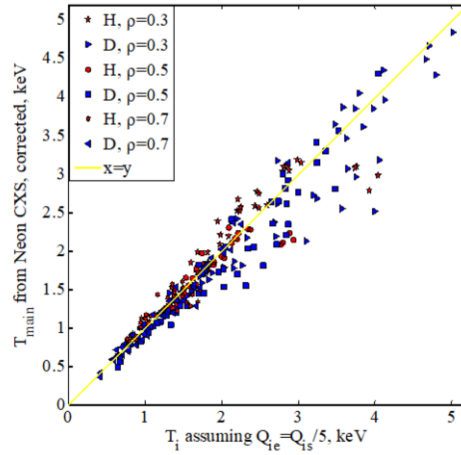


Fig.5 Main ion temperatures from CXS plotted against $T_{\text{ieq}}(f_i=0.2,\rho)$ for three radial positions, showing $T_i(\rho)\approx T_{\text{ieq}}(f_i=0.2,\rho)$.

3.1. Global thermal energy confinement in H-mode

The thermal stored energy is calculated as

$$W_{\text{th}} = 1.5eI(n_e(\rho)T_e(\rho) + n_i(\rho)T_{\text{ieq}}(f_i=0.2,\rho))dV(\rho) \quad (\text{eq.1}), \text{ where } n_i \text{ is estimated as}$$

$$n_i = n_e - (Z-1)n_z = n_e(1 - (Z_{\text{eff}}-1)/Z),$$

with $Z=4$, i.e. with the assumption that Be is the main impurity. JET-ILW plasmas are of high purity with the bulk of the data presented having $1.05 < Z_{\text{eff}} < 1.6$, as inferred from visible Bremsstrahlung measurements for this H-mode dataset. As a result, errors on n_i/n_e inferred by assuming a single impurity species are small ($< 10\%$). The regression for W_{th} is shown in fig.6 and given below:

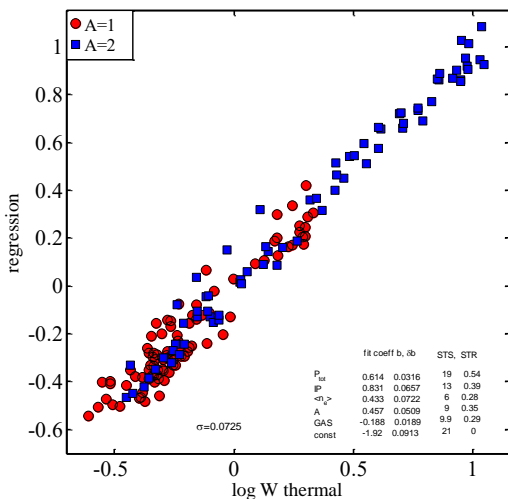


Fig.7 Regression for stored thermal energy confinement assuming $T_{\text{main}}(\rho)=T_{\text{ieq}}(f_i=0.2,\rho)$,

$$W_{\text{th}} \propto A^{0.46 \pm 0.06} P^{0.61 \pm 0.03} I_p^{0.83 \pm 0.07} \langle n_e \rangle^{0.43 \pm 0.08} G^{-0.19 \pm 0.02} \quad \text{with}$$

$$\sigma / \log(W_{\text{thmax}} / W_{\text{thmin}}) = 0.044 \quad (\text{reg.1})$$

P is the total absorbed power, $\langle n_e \rangle$ the volume averaged density, G the gas puff rate and s the standard deviation of the regression in log space, W_{thmax} and W_{thmin} are the extremal values of W_{th} in the dataset. In type I ELMy deuterium H-modes in JET-ILW the density cannot be effectively controlled by gas puffing, however in hydrogen it can. Confinement degrades with increasing gas rate, making G a better regression variable in deuterium than $\langle n_e \rangle$. This is why the best regressions are obtained by including both $\langle n_e \rangle$ and G as variables. When G is not included (as in IPB98(y,2) [3]) a regression of lesser quality and a likely excessively strong mass dependence is obtained:

$$W_{\text{th}} \propto A^{0.63 \pm 0.08} P^{0.57 \pm 0.05} I_p^{0.9 \pm 0.11} \langle n_e \rangle^{0.008 \pm 0.1}$$

$$\text{with } \sigma / \log(W_{\text{thmax}} / W_{\text{thmin}}) = 0.076 \quad (\text{reg.2})$$

We have also inferred the thermal stored energy from the EFIT equilibrium reconstruction, corrected for the fast ion contribution, providing the regression

$$W_{\text{th-EFIT}} \propto A^{0.39 \pm 0.06} P^{0.64 \pm 0.04} I_p^{0.88 \pm 0.09} \langle n_e \rangle^{0.5 \pm 0.11} G^{-0.21 \pm 0.025} \quad \text{with } \sigma / \log(W_{\text{th-EFITmax}} / W_{\text{th-EFITmin}}) = 0.054 \quad (\text{reg.3})$$

Regression reg.1 & 2 have similar isotope dependencies as reported in [1], where $W_{\text{th}} \propto A^{0.4}$ was found assuming $T_i = T_e$.

The effect of H/D mixtures was explored in a systematic scan of the H/(H+D) ratio at $P_{\text{TOT}} \sim 10\text{-}13\text{MW}$ in type I ELMy H-mode at 1.4MA/1.7T. These show a regular decrease of stored energy from $W_{\text{th}} \sim 1.4\text{MW}$ in deuterium to $\sim 1.1\text{MW}$ in hydrogen. At this power level, in pure hydrogen, a type I ELMy regime was not always achieved. Instead, these plasmas had type III ELMs and $W_{\text{th}} \sim 0.8\text{MW}$.

3.2. Global momentum confinement in H-mode

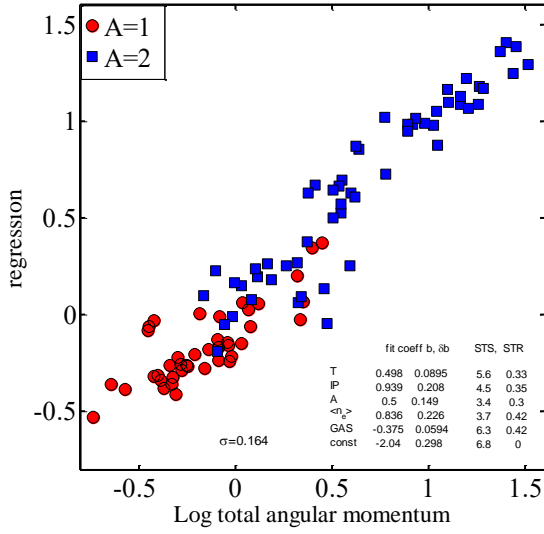


Fig.7 Regression for the stored angular momentum

$$L_\phi \propto A^{0.5 \pm 0.15} T^{0.5 \pm 0.09} I_p^{0.94 \pm 0.21} \langle n_e \rangle^{0.84 \pm 0.23} G^{-0.38 \pm 0.06} \quad \text{with } \sigma / \log(L_\phi \text{ max} / L_\phi \text{ min}) = 0.08 \quad (\text{reg.4})$$

Here T is the NBI torque. Momentum confinement has a significantly stronger dependence on the gas fuelling rate than energy confinement, possibly as a result of increasing charge exchange losses with increasing edge neutral densities.

3.3. Global particle confinement in H-mode

Particle confinement has been estimated by using both the divertor and main chamber Balmer alpha emission, together with the NBI beam fuelling rate, as proxies for the particle source. At same injected gas rate, hydrogen plasmas achieved densities which were typically a little over half as high as their deuterium counterparts. Similar densities were only achieved in a few cases and required several times stronger gas puffing in hydrogen. The best regressions for the total electron content $N_e = \int n_e dV$ are obtained with the divertor Balmer alpha emission as a proxy for the particle source:

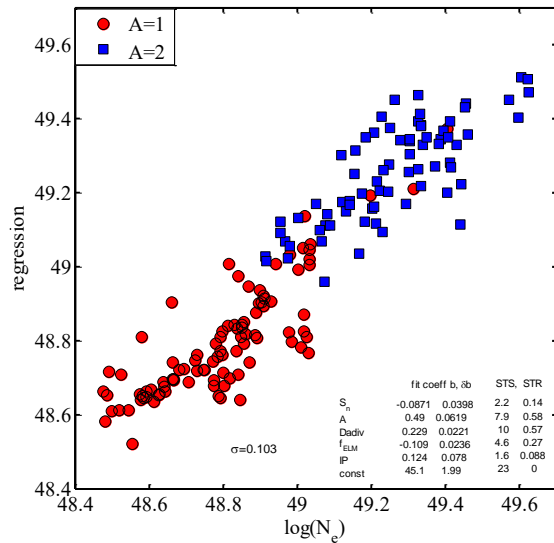


Fig.8 Regression for total electron content

$$N_e \propto A^{0.49 \pm 0.06} \Gamma_{div}^{0.23 \pm 0.022} f_{ELM}^{-0.11 \pm 0.024} S_{NBI}^{-0.08 \pm 0.04} I_p^{0.12 \pm 0.08} \text{ with } \sigma/\log(N_{e \max}/N_{e \min}) = 0.09 \quad (\text{reg.5})$$

Here f_{ELM} is the ELM frequency and S_{NBI} is the beam fuelling rate calculated using PENCIL [6]. While the mass exponent is very close to the ones found for momentum and thermal energy, the other dependencies are intriguing. ELMs reduce particle confinement in type I low triangularity H-modes. At first sight, beam fuelling seems unimportant. However as $S_{NBI} \propto P_{NBI}$ the weak and negative dependency may simply result from competition between fuelling and transport. The essential role of edge fuelling is however evident from the fact that no successful regression is obtained when no proxy for the edge source is included. Most intriguingly, the dependence on I_p is very weak, unlike for momentum and energy confinement.

3.4. Pedestal stability and transport

Since core temperature profiles are essentially stiff (small variations of R/L_T for large variations in the heat flux)

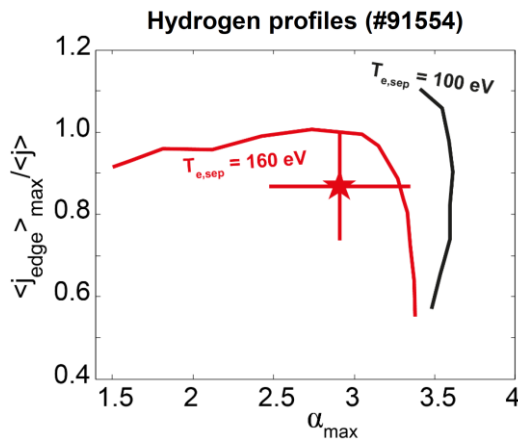


Fig.9 Peeling-ballooning stability diagrams, showing shrinkage of the stable region at elevated separatrix temperature.

maximum of the pressure gradient closer to the LCFS, leading to a shrinkage of the peeling-ballooning boundary towards the experimentally observed existence point, as seen in fig.9. The higher temperature in hydrogen may itself be a consequence of the lower density in hydrogen and a consequence of transport processes. The determination of the separatrix temperature and density is, unfortunately, experimentally challenging.

Type I ELM frequencies are higher in hydrogen than in deuterium at the same power to the separatrix and gas rate. The pedestal top density depends clearly on ELM frequency, as seen in fig. 10, suggesting that the more frequent ELMs also contribute to lowering the density in hydrogen. However, at ELM frequencies above 40Hz the estimated time-averaged particle losses $\Delta N_e f_{ELM}$ become independent of both f_{ELM} and the isotope species. Hence ELMs alone cannot be the only reason for lower densities in hydrogen [15].

pedestal conditions are most likely at the origin of the isotope effect manifested throughout the plasma. HELENA/ELITE stability calculations [12,13] show that pedestals in both species are broadly consistent, at low gas rates, with the peeling-ballooning paradigm [14], with hydrogen pedestals being somewhat more on the stable side of the boundary [15]. The stability criterion $\gamma_{MHD} > 0.5 \omega_{DIA}$, where $\gamma_{MHD} \propto A^{-1/2}$, leads to a modest shift of the stability boundary towards lower values of α for hydrogen with respect to deuterium. This would translate only to a $\sim 5\%$ reduction in pedestal pressure, assuming operation at the stability boundary, which is much weaker than seen in the experiment. Hence the differences in pedestal pressure and overall confinement appear not to be limited by peeling-ballooning stability of the pedestal. There may however be an indirect effect on pedestal stability if separatrix temperatures are confirmed to be higher in hydrogen, as EDGE2D-EIRENE simulations suggests. A stability calculation with a separatrix electron temperature of 160 eV (instead of 100eV in deuterium) had the

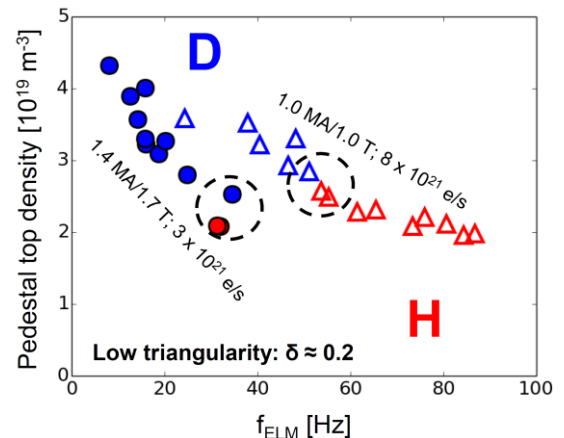


Fig.10 Pedestal top density scaling with ELM frequency

The necessity for stronger fuelling in hydrogen is at odds with popular conceptions of fuelling by neutral penetration, as for all other parameters being equal (e.g. T_i), hydrogen neutrals should penetrate deeper into the plasma, thanks to their greater thermal velocity. The observation suggests that transport processes in the pedestal may overcome the effect of thermal velocity. The pedestal width model [16] based on neutral penetration is also not consistent with observations of hydrogen and deuterium pedestals [15]. This model [16] predicts a pedestal width scaling as

$$\Delta_{ne} \propto A^{-1/2} (T_{iped}/T_{eped})^{-1/2} n_{eped}^{-1}.$$

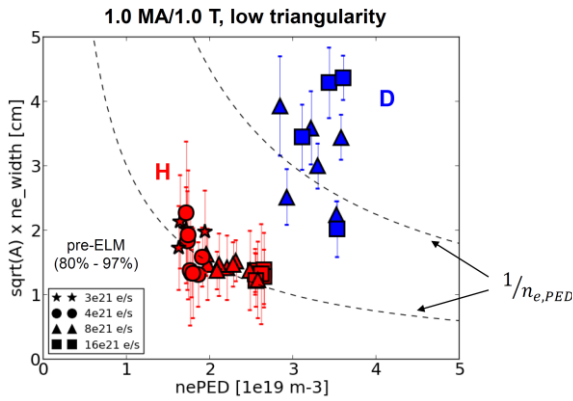


Fig.11 Measured pedestal density width compared with scaling from [11] for the 1MA subset. The symbols refer to the gas injection rate.

In the 1MA/1T subset the measured widths, taken shortly before the ELM crashes, deviate by a factor two from the scaling (fig.11). At 1.4MA/1.7T, at higher gas rate, there is no clear dependence of Δ_{ne} on species, nor on n_{eped} [15]. EDGE2D EIRENE was used to model the plasma boundary and pedestal region of a pair of H-modes in the two species. Both required a transport barrier to model the pedestal and near SOL of 3cm width. In hydrogen the required particle diffusion coefficient was as much as 5 times higher than in deuterium. When only the isotope was changed to hydrogen in a simulation for deuterium, there was only a modest change in T_e and n_e profiles, which was opposite in sign to the observations. The analysis shows that plasma density profiles in the boundary are governed also by particle transport processes and are more complex than expected from neutral fuelling physics only.

3.5. Non-linear gyrokinetic simulations

A pair of hydrogen and deuterium discharges with same heating power (10MW) from the type I ELMy H-mode dataset has been analysed with flux-tube simulations at $\rho=0.5$ using the gyrokinetic code GENE [17]. These simulations were done for both species for each of the two discharges [18]. Linear simulations including the effect of collisions show no significant deviations from Gyro-Bohm scaling. Nonlinear simulations reproduce the observed heat fluxes (with a slight overprediction) if R/L_{T_e} is reduced by 20% in the hydrogen discharge and 17% in the deuterium discharge, collisions and $E \times B$ shear are included and dilution by Be is accounted for (fig.12). All of these effects are seen to break Gyro-Bohm scaling locally at $\rho=0.5$. Collisions suppress TEM modes and are essential for obtaining realistic heat fluxes. Including $E \times B$ shear reduces the heat flux in for deuterium but not for hydrogen.

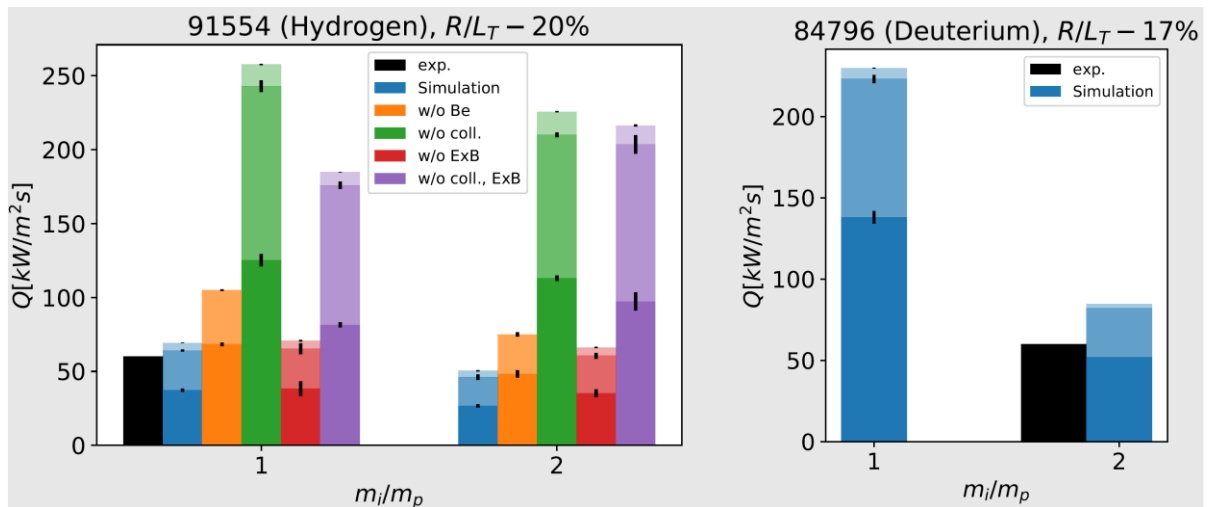


Fig.12 Heat fluxes obtained for various non-linear GENE flux tube simulations. Left: hydrogen H-mode plasma simulated for $A=1$ and $A=2$, including different effects. Right: deuterium plasma. The transparency of the bars codes for species contributions: main ions, electrons and Be impurities (from bottom to top of bars).

Collisions have a strong effect on the zonal flow shearing rate $\omega_{E \times B}$ spectra, which were evaluated for the profiles in the hydrogen case. With collisions included, spectra for deuterium are shifted towards lower $k_{\theta} \rho_s$ with respect to the hydrogen case. The RMS average $\omega_{E \times B}$ for deuterium is slightly lower than for hydrogen when collisions are neglected, but is slightly larger in the collisional simulations. This is in qualitative agreement with the differences in heat fluxes. These non-linear GENE simulations show that reversal of GyroBohm scaling is to be expected and explain the observed heat fluxes with fair quantitative agreement. This is highly encouraging, but we should keep in mind that we cannot extrapolate to global scaling from any local core transport model alone. It is quite possible that in global nonlinear simulations with experimentally imposed boundary conditions, e.g. at the top of the pedestal, the global confinement will be strongly dependent on the boundary conditions as a result of profile stiffness.

4. CONCLUSIONS

Following the results reported in [1], progress in data analysis and modelling has confirmed the scalings of the global energy confinement with isotope mass in L-mode (weak) and H-mode (strong) and extended them to include the momentum and the particle confinement. The latter has a weak scaling with mass in L-mode too. Remarkably, in H-mode all three transport channels, energy, momentum and particle transport, have similar isotope scalings, with mass exponents around 0.4 to 0.5. As a result of the observed and modelled temperature profile stiffness, the origin of global isotope scaling is sought for in the physics of the pedestal, which is sensitive to recycling and atomic physics processes. Analysis of density pedestal width shows that neutral fuelling physics alone is insufficient to explain the systematic differences between the species, pointing to the importance of transport processes in the pedestal that are species dependent and still to be understood. Core confinement is hostage to pedestal conditions as a result of stiff temperature profiles in ITG dominated turbulence. This causes local GyroBohm scaling to be overridden in JETTO-TGLF simulations in L-mode, resulting in a prediction of independence of confinement on the isotope species. In non-linear flux-tube GENE simulations of the core of H-modes GyroBohm scaling is even reversed by the effect of collisions, $\omega_{E \times B}$ shear and impurities. The lessons from modelling work so far is that several effects can break GyroBohm scaling for global confinement and therefore experimental results showing anti-GyroBohm scaling of global confinement are not incompatible with local GyroBohm scaling. This work underscores that an understanding of the pedestal and SOL physics is key to understanding overall tokamak confinement and transport.

ACKNOWLEDGEMENTS

This work has been carried out within the framework of the EUROfusion Consortium and has received funding from the Euratom research and training programme 2014-2018 under grant agreement No 633053. The views and opinions expressed herein do not necessarily reflect those of the European Commission.

REFERENCES

- [1] C.F. Maggi et al, Plasma Physics and Controlled Fusion **60** (2018) 014045
- [2] I. M. F. Nunes et al, 26th IAEA FEC, Kyoto, 2016, IAEA CN-234, [PDP-2, EXC-P8](#)
- [3] ITER Physics Basis, Nuclear Fusion **39** (1999) 2175
- [4] C.F. Maggi et al, 45th EPS Conference on Plasma Physics, Prague, 2018, to be submitted to Nuclear Fusion
- [5] T.C. Luce et al, Plasma Phys. Control. Fusion **50** (2008)
- [6] Challis C C et al 1989 Nucl. Fusion 29 563
- [7] M.J. Mantsinen et al., Plasma Phys. Control. Fusion 41 (1999) 843.
- [8] Staebler G et al. 2007 Phys. Plasmas **14** 055909
- [9] M. Romanelli et al (2014) Plasma and Fusion Research **9**, 3403023
- [10] Cordey J G et al. 2000 Plasma Phys. Control. Fusion **42** A127
- [11] H. Weisen et al., 40th EPS Conference on Plasma Physics, Espoo, 2013, [P2.131](#)
- [12] Huysmans G T A, et al, 1991 Proc. Int. Conf. on Comp. Physics (Amsterdam, 1990) (Singapore: World Scientific) p 371
- [13] Wilson H R, et al, 2002 Phys. Plasmas **9** 1277
- [14] P.B. Snyder et al, [Phys. Plasmas **9** \(2002\) 2037](#)
- [15] L. Horvath et al, to be submitted to Nuclear Fusion
- [16] Groebner R.J. et al 2002 Phys. Plasmas **9** 2134
- [17] <http://genecode.org/>
- [18] M. Oberparleiter et al, to be submitted for publication